

EventFormer: AU Event Transformer for Facial Action Unit Event Detection

Yingjie Chen, Jiarui Zhang, Tao Wang*, Yizhou Wang, and Yun Liang

Abstract—Facial action units (AUs) play an indispensable role in human emotion analysis. We observe that although AU-based high-level emotion analysis is urgently needed by real-world applications, frame-level AU results provided by previous works cannot be directly used for such analysis. Moreover, as AUs are dynamic processes, the utilization of global temporal information is important but has been gravely ignored in the literature. To this end, we propose EventFormer for AU event detection, which is the first work directly detecting AU events from a video sequence by viewing AU event detection as a multiple class-specific sets prediction problem. Extensive experiments conducted on a commonly used AU benchmark dataset, BP4D, show the superiority of EventFormer under suitable metrics.

I. INTRODUCTION

Facial expression, as the most expressive emotional signal, plays an essential role in human emotion analysis. According to Facial Action Coding System (FACS) [1], facial action units (AUs) refer to a set of facial muscle movements and are the basic components of almost all facial behaviors. The increasing need for user emotion analysis in application scenarios, such as online education and remote interview, leads to rapid growth in the field of AU analysis in recent years. With the prosperity of deep learning, two mainstream tasks of AU analysis, AU recognition [2], [3], [4] and AU intensity estimation [5], [6], [7], have seen great improvements in recent years, both of which aim to predict frame-level AU occurrences.

However, when it comes to high-level emotion analysis, frame-level analysis results are not enough for the need of some real-world applications [8], [9], due to the lack of various sequence-level information for further analysis, such as the occurrence frequencies, durations, and chronological order of AU events, each of which is a temporal segment containing one AU’s complete temporal evolution, as shown in Fig. 1. For example, in public places such as airports, unnatural facial expressions or fleeting panics act as key information for the discrimination of a suspicious passenger. In this case, sequence-level AU event results are required to capture such abnormal emotions and based on which, warnings will be sent to officers for a further inspection of the person. Furthermore, sequence-level AU event results are also important for the distinction between spontaneous and pretended facial expressions. For *happiness*, the identification depends heavily on the overlapping situation of events

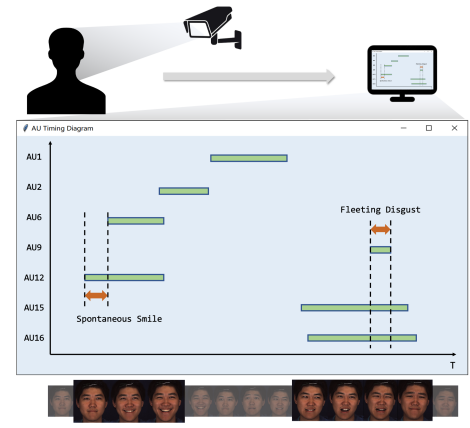


Fig. 1. An illustration of the potential application scenario of direct sequence-level AU event detection. AU event provides overlapping as well as chronological information between different AUs, which is more suitable for further emotion analysis.

labeled AU6 and AU12, in which case not only AU events’ durations but also their chronological order matters.

Some works [10], [11] have made attempts to generate AU event results based on frame-level or unit-level (a fixed number of frames centered on the current one is regarded as a unit) AU results via a series of postprocessing steps, but they suffer from the lacking of global temporal information and are highly dependent on hyper-parameters for postprocessing. To this end, we design an AU **Event TransFormer (EventFormer)** architecture to directly detect AU events from a video sequence by utilizing the benefit of global temporal information. EventFormer takes a video sequence as input and detects AU events for each AU class directly and simultaneously by viewing AU event detection as a *multiple class-specific sets prediction problem*.

Specifically, first, a region-aware AU feature encoder is used for extracting fine-grained AU features as frame embedding. Then, an event transformer encoder-decoder module is used to generate event embeddings by learning global dependencies among frames in a video sequence. Through self-attention mechanism, all frame embeddings are fed to transformer architecture simultaneously, and each frame can interact with others directly. In this way, a global view is maintained. After that, classification branch and regression branch are applied to each event embedding for event validity prediction and boundary regression, respectively.

Unlike methods such as [12] modeling local temporal relations among several frames via RNN [13] or methods such as [11], [14] using local temporal information by ex-

* Corresponding author

The authors are with the School of Computer Science, Peking University, Beijing 100871, China, e-mail: {chenyingjie, zjr954, wangtao, yizhou.wang, ericlyun}@pku.edu.cn

tracting unit-level features, our EventFormer takes the whole video sequence as input and model global temporal relations through the mechanism of transformer, which allows each frame to access all the other frames simultaneously. And instead of generating AU events based on frame-level results through postprocessing which highly depends on manually selected hyper-parameters, EventFormer detects AU events in a direct way, and thus is able to alleviate discontinuous results.

The key contributions of our work are listed as:

- To the best of our knowledge, this is the first work that directly detect AU events from a video sequence, which are more critical and practical for real-world applications.
- We propose EventFormer for AU event detection, which takes advantage of the mechanism of transformer to maintain a temporal global view and alleviate discontinuous results.
- Extensive experiments conducted on a commonly used AU benchmark dataset, BP4D, show the superiority of the proposed method under suitable metrics for AU event detection.

II. RELATED WORK

In recent years, AU analysis tasks have drawn increasing attention as fundamental tasks in the field of affective computing. Conventional methods [15], [14] mainly design hand-crafted features as the input of a classifier for AU recognition. With the development of deep learning, methods [16], [12], [17] have raised the performance of AU analysis to a new height. Since AUs are dynamic processes, methods such as [12] employ LSTM to model local temporal relations, but fail in extending to longer temporal range. To obtain AU event results, Ding *et al.* [11] proposed a method that extracts unit-level features, predicts event-related scores and generates AU events via a series of postprocessing steps. In contrast, we propose EventFormer to model global temporal relations among frames in a video sequence and detect AU events in a direct way.

Transformer [18] has attracted increasing research interest in computer vision tasks. Self-attention mechanism as the core of transformer allows the model to aggregate information from the whole input sequence with much less memory consumption and computing time compared to RNNs. However, it is not until works [19], [20] succeeded that the architecture has been proved effective and efficient in computer vision tasks. Our EventFormer makes full use of the mechanism to model global temporal information.

III. EVENTFORMER FOR AU EVENT DETECTION

A. Problem Definition

Given an input video sequence $\mathcal{I} = \{I_t\}_{t=1}^T$ with T frames recording facial actions, where I_t is the t^{th} frame in \mathcal{I} . The annotations of \mathcal{I} are composed of a set of ground-truth AU events $\Phi_g = \{\phi_i = (s_i^g, e_i^g, c_i^g) | 0 \leq s_i^g < e_i^g \leq T, c_i^g \in \{1, 2, \dots, C\}\}_{i=1}^M$, where M is the number of ground-truth AU events in the video sequence \mathcal{I} , C is the number

of AU classes, and s_i^g, e_i^g, c_i^g are the start time, end time, and AU class label of AU events ϕ_i , respectively. AU event detection aims to detect a set of events $\Phi_p = \{\varphi_i = (s_i^p, e_i^p, c_i^p) | 0 \leq s_i^p < e_i^p \leq T, c_i^p \in \{1, 2, \dots, C\}\}_{i=1}^N$ which match Φ_g precisely and exhaustively. During training, the set of ground-truth AU events Φ_g is used as supervision for detected events Φ_p , and during inference, the Φ_p can be simply filtered as results.

B. Multiple Class-specific Sets Prediction

Due to AU co-occurrence relationships, AU events in different AU classes can have near-identical or exactly identical temporal boundaries. Inspired by DETR [20] which views object detection as a single set prediction problem, we view AU event detection as a multiple class-specific sets prediction problem. Instead of predicting a class-agnostic set with events of all classes, we predict multiple class-specific sets, each set contains events for a specific AU class.

As noted above, AU event detection aims to detect class-specific sets of AU events, $\Phi_p = \{\varphi_i = (s_i^p, e_i^p, c_i^p)\}_{i=1}^N$, from a video sequence \mathcal{I} . If we bind AU class labels to events and search for a permutation of Φ_p to match Φ_g directly, some class mismatches caused by the multi-label property of AU event detection are hard to solve. For example, events with identical temporal boundaries but different AU class labels in Φ_g can match with any permutation of the corresponding detected events in Φ_p during training, which causes unstable training and makes the class labels hard to learn. To alleviate the instability issue, we split Φ_g into C disjoint class-specific sets $\{\Phi_g^c\}_{c=1}^C$ such that $\Phi_g = \bigcup_{c=1}^C \Phi_g^c$, where $\Phi_g^c = \{\phi_i^c = (s_i^g, e_i^g, c_i^g) | \forall \phi_i \text{ s.t. } c_i^g = c\}_{i=1}^{N_c}$, and N_c is the number of ground-truth events belonging to class c . In this way, the problem turns into predicting several class-specific sets Φ_p^c , ($\Phi_p = \bigcup_{c=1}^C \Phi_p^c$), one for each AU class, *i.e.* a multiple class-specific sets prediction problem.

For the implementation of EventFormer, assuming N_0 is a number larger than any N_c , we pad Φ_g^c with \emptyset (no event) to make the set $\tilde{\Phi}_g^c = \{\tilde{\phi}_i^c = (s_i^g, e_i^g, \tilde{c}_i^g)\}_{i=1}^{N_0}$ with a fixed number of events, where $\tilde{c}_i^g \in \{0, 1\}$, $\tilde{c}_i^g = 0$ represents $\tilde{\phi}_i^c$ is not a valid event, *i.e.* \emptyset for padding, and $\tilde{c}_i^g = 1$ represents $\tilde{\phi}_i^c$ is a valid event. We denote $\tilde{\Phi}_p^c = \{\tilde{\varphi}_i^c = (s_i^p, e_i^p, \tilde{c}_i^p)\}_{i=1}^{N_0}$ as the set of N_0 detected events for class c , called *Event Set c*. EventFormer takes a video sequence \mathcal{I} and a union of C *Query Sets* $\Phi_q = \bigcup_{c=1}^C \Phi_q^c$ as inputs, and outputs a union of C corresponding *Event Sets* $\tilde{\Phi}_p = \bigcup_{c=1}^C \tilde{\Phi}_p^c$.

C. EventFormer Architecture

As shown in Fig. 2, our EventFormer mainly consists of three parts.

1) *AU Feature Encoder*: Compared to coarse-grained body actions, AUs only cause subtle appearance changes on several local facial regions, which puts high demands on the discriminability of frame embeddings. Thus, we design a region-aware AU feature encoder to extract local features for each AU separately to preserve more detailed information. Each frame $I_t \in \mathbb{R}^{3 \times H \times W}$ in \mathcal{I} is fed to a backbone network to extract $F^{\text{global}} \in \mathbb{R}^{d \times H_0 \times W_0}$ as global feature.

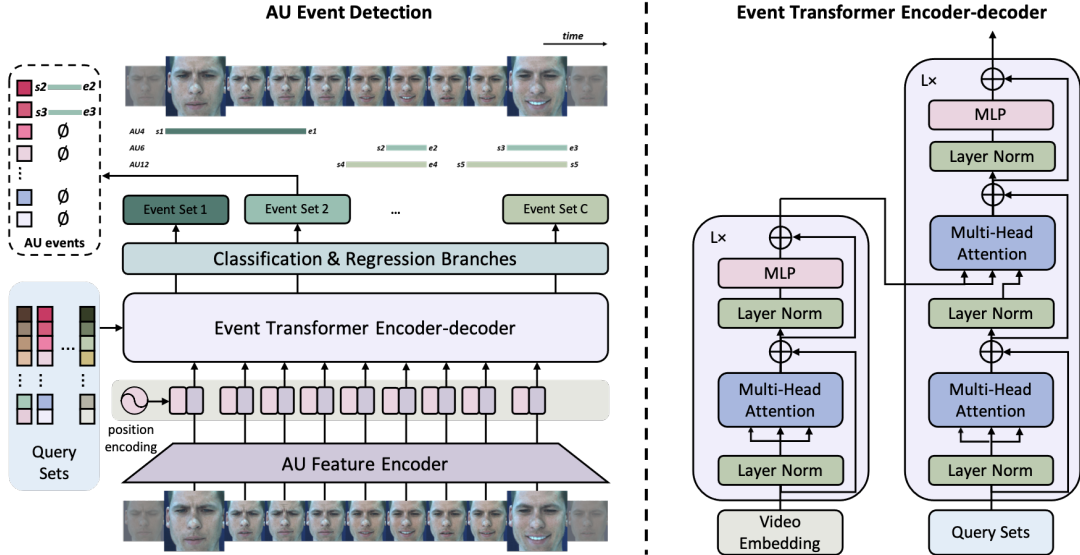


Fig. 2. Architecture of EventFormer. EventFormer takes a video sequence as input, and AU feature encoder is first applied to the input to generate frame embeddings. Then position embeddings are concatenated to each frame embedding as the input of event transformer encoder-decoder module. Event transformer encoder models global relationships among frames via self-attention mechanism to enhance frame embeddings. After that, event transformer decoder takes encoder output and sets of queries, *i.e.* *Query Sets*, as input, and outputs aggregated event embeddings for each query. Then the output event embeddings are passed to two branches to obtain the final *Event Sets*.

And C spatial attention layers [21] are applied to the global feature to extract local features $f^{\text{local}} \in \mathbb{R}^d$ for each AU (Details in Supp.A). Then, the concatenated local features $F^{\text{local}} \in \mathbb{R}^{(d \times C)}$ are mapped to $E_t \in \mathbb{R}^{d_m}$ via a linear layer as frame embedding for I_t .

2) *Event Transformer Encoder-decoder Module*: We start from the original transformer encoder-decoder architecture [18] and design an event transformer encoder-decoder module specially for AU event detection. Preliminaries of transformer are provided in Supp.B. Our event transformer encoder-decoder consists of L encoder layers and L decoder layers. To ensure a stable training period, LayerNorm [22] is applied before Multi-head Attention and Multi-layer Perceptron, according to [23]. To maintain positional information in time dimension, positional encoding is employed to generate positional embeddings $\mathcal{P} = \{P_t\}_{t=1}^T \in \mathbb{R}^{T \times d_m}$, corresponding to frame embeddings $\mathcal{E} = \{E_t\}_{t=1}^T \in \mathbb{R}^{T \times d_m}$ (Details in Supp.B.3). The transformer encoder takes the concatenated frame embeddings and positional embeddings, *i.e.* video embedding, as input and outputs refined frame embeddings by enabling interaction among frames via self-attention mechanism. Event transformer decoder takes event queries $Q \in \mathbb{R}^{(CN_0) \times d_m}$ as input, which can be regarded as the union of C *Query Sets*, $\Phi_q = \bigcup_{c=1}^C \Phi_q^c$, where $\Phi_q^c = \{q_i^c\}_{i=1}^{N_0}$. Each query $q_i^c \in \mathbb{R}^{d_m}$ is a learned positional embedding, which differs from each other. Queries first interact with each other through self-attention to alleviate event redundancy, and then interact with the encoder output, *i.e.* the refined frame embeddings as keys and values, to aggregate frame embeddings relative to each potential event as event embeddings $D \in \mathbb{R}^{(CN_0) \times d_m}$.

3) *Classification and Regression Branches*: The output event embeddings D of the event transformer encoder-decoder module are further fed into classification branch and regression branch separately. For each feature vector $d_i \in \mathbb{R}^{d_m}$ in D representing a potential event φ_i , the regression branch aims to estimate the start time s_i and duration l_i of the event, and $e_i = \min(T, s_i + l_i)$. The classification branch aims to estimate a one-hot vector $\hat{p}_i \in \mathbb{R}^2$ that denotes the probabilities of the value of \tilde{c}_i . We use a linear layer to output the classification probability \hat{p}_i and two linear layers to regress s_i and l_i . After that, by reorganizing events in order, $\tilde{\Phi}_p = \bigcup_{c=1}^C \tilde{\Phi}_p^c$ is obtained.

IV. TRAINING AND INFERENCE OF EVENTFORMER

To train EventFormer, a multiple class-specific sets matching cost is introduced for class-specific bipartite matching between each pair of $\tilde{\Phi}_g^c$ and $\tilde{\Phi}_p^c$. After the matching for each AU class, a multiple class-specific sets prediction loss can be computed for back-propagation.

A. Multiple Class-specific Sets Matching Cost

Due to the disorder of events in one set, the loss function designed for multiple class-specific sets prediction should be invariant by a permutation of the detected events with identical class labels, *i.e.* in one *Event Set*. We apply a loss based on Hungarian algorithm [24], to find a bipartite matching between ground-truth events and detected ones for each class.

A permutation of N_0 elements $\sigma \in \Omega_{N_0}$ is searched by finding a bipartite matching between $\tilde{\Phi}_g^c$ and $\tilde{\Phi}_p^c$ for each class that minimizes the total matching cost, as shown in

Eq. 1:

$$\hat{\sigma} = \arg \min_{\sigma \in \Omega_{N_0}} \sum_{i=1}^{N_0} \mathcal{L}_{\text{match}}(\tilde{\phi}_i^c, \tilde{\varphi}_{\sigma(i)}^c), \quad (1)$$

where $\mathcal{L}_{\text{match}}(\tilde{\phi}_i^c, \tilde{\varphi}_{\sigma(i)}^c)$ is a pair-wise matching cost between ground-truth $\tilde{\phi}_i^c$ and a detected event $\tilde{\varphi}_{\sigma(i)}^c$ with matching index $\sigma(i)$. The loss function of matching is designed to minimize the distance between matched pairs and maximize the validity of matched events at the same time. We define $\mathcal{L}_{\text{match}}(\tilde{\phi}_i^c, \tilde{\varphi}_{\sigma(i)}^c)$ as

$$\mathbb{1}_{\{\tilde{c}_i^g=1\}} \left(\lambda_{\text{bound}} \mathcal{L}_{\text{bound}}(\tilde{\phi}_i^c, \tilde{\varphi}_{\sigma(i)}^c) - \lambda_{\text{valid}} \hat{p}_{\sigma(i)}^c[\tilde{c}_i^g] \right), \quad (2)$$

where $\hat{p}_{\sigma(i)}^c \in \mathbb{R}^2$ denotes the probabilities of the value of $\tilde{c}_{\sigma(i)}^p$ indicating whether $\tilde{\varphi}_{\sigma(i)}^c$ is a valid event, *i.e.* the probabilities of $\tilde{c}_{\sigma(i)}^p \in [0, 1]$, $\hat{p}_{\sigma(i)}^c[\tilde{c}_i^g]$ denotes the probability of $\tilde{c}_{\sigma(i)}^p = \tilde{c}_i^g$, and λ_{bound} and λ_{valid} are for balancing. The boundary loss $\mathcal{L}_{\text{bound}}$ measures the similarity between a pair of matched ground-truth event and detected event. L1 loss measures the numerical difference of the regression results, and tIoU loss measures the overlapping area ratio of matched pairs. Both of them are used, considering pairs of ground-truth event and detected event may have a minor difference in terms of L1 but a huge difference in terms of tIoU. Thus, a linear combination of tIoU loss (Eq. 3) and L1 loss is used as our boundary loss $\mathcal{L}_{\text{bound}}$, as shown in Eq. 4.

$$T_{\cap} = \max(0, \min(e_1, e_2) - \max(s_1, s_2)),$$

$$\mathcal{L}_{\text{tIoU}}((s_1, e_1), (s_2, e_2)) = \frac{T_{\cap}}{(e_1 - s_1) + (e_2 - s_2) + T_{\cap}}. \quad (3)$$

$$\begin{aligned} \mathcal{L}_{\text{bound}}(\tilde{\phi}_i^c, \tilde{\varphi}_{\sigma(i)}^c) &= \lambda_{\text{tIoU}} \mathcal{L}_{\text{tIoU}}((s_i^g, e_i^g), (s_{\sigma(i)}^p, e_{\sigma(i)}^p)) \\ &+ \lambda_{\text{L1}} (\|s_i^g - s_{\sigma(i)}^p\| + \|e_i^g - e_{\sigma(i)}^p\|), \end{aligned} \quad (4)$$

where λ_{tIoU} and λ_{L1} are for balancing.

B. Multiple Class-specific Sets Prediction Loss

After finding a bipartite matching minimizing the matching cost, the loss function can be computed. A combination of $\mathcal{L}_{\text{bound}}$ and $\mathcal{L}_{\text{class}}$ (Eq. 5) forms the event detection loss \mathcal{L} , as shown in Eq. 6.

$$\mathcal{L}_{\text{class}}(p_i^c, \hat{p}_{\sigma(i)}^c) = - \sum_{\tilde{c} \in (0, 1)} p_i^c(\tilde{c}) \log(\hat{p}_{\sigma(i)}^c(\tilde{c})). \quad (5)$$

$$\begin{aligned} \mathcal{L} &= \sum_{c=1}^C \sum_{i=1}^{N_0} (\mathbb{1}_{\{\tilde{c}_i^g=1\}} \mathcal{L}_{\text{bound}}(\tilde{\phi}_i^c, \tilde{\varphi}_{\sigma(i)}^c) \\ &+ \lambda_{\text{class}} \mathcal{L}_{\text{class}}(p_i^c, \hat{p}_{\sigma(i)}^c)), \end{aligned} \quad (6)$$

where $p_i^c \in \mathbb{R}^2$ is the one-hot encoding of \tilde{c}_i^g for $\tilde{\phi}_i^c$ and λ_{class} is for balancing. It is worth mentioning that all the detected events are involved in the calculation of $\mathcal{L}_{\text{class}}$, but only the matched events in *Event Sets* are involved in the calculation of $\mathcal{L}_{\text{bound}}$.

In the inference stage, bipartite matching is disabled. By given a threshold τ , we can simply filter out events with $\hat{p}_i[1]$ lower than the threshold and preserve more valid events. For each *Event Set* c , each preserved event $\tilde{\varphi}_i^c$ is assigned

with an AU class label c to form one final detected event $\varphi_i = (s_i^p, e_i^p, c_i^p)$ with $c_i^p = c$ in Φ_p . In this way, the set of final AU events Φ_p can be easily obtained.

V. EXPERIMENTS

A. Experimental Settings

1) *Datasets & Metrics*: Extensive experiments are conducted on a commonly used benchmark dataset, BP4D [25]. In BP4D, 328 videos of 41 participants are taken, including 23 women and 18 men. Each frame is annotated by certified FACS coders with binary AU occurrence labels. We consider 12 emotion-related AUs on BP4D, including AU1, 2, 4, 6, 7, 10, 12, 14, 15, 17, 23 and 24. To construct the training data, we use a sliding window with length T to truncate all the videos into several equal length video sequences, and there is an overlap of $T/2$. Based on binary AU occurrence labels, ground-truth AU events Φ_g are obtained for each video sequence. Following the common protocol mentioned in [16], subject-exclusive 3-fold cross-validation is conducted for all experiments.

Considering that AU event detection shares some similarities with temporal action detection [26], we select several suitable metrics for AU event detection drawing on those used in that task. The goal of AU event detection task is to detect AU events with not only high precision but also acceptable recall. Thus, we consider Mean Average Precision(mAP) and Average Recall with an average number of events (AR@AN) at different tIoU thresholds α . α is set to $[0.3 : 0.1 : 0.7]$ for mAP and $[0.5 : 0.05 : 0.95]$ for AR@AN. We also report Area under the AR vs. AN curve (AUC) for evaluation.

2) *Implementation Details*: Facial images are cropped and resized to 256×256 . ResNet50 [27] without the last linear layer is used as backbone in AU feature encoder. Empirically, we set local feature dimension $d = 512$, $H_0 = W_0 = 16$, embedding dimension $d_m = 256$, and the number of encoder/decoder layers L is set to 6. Other hyper-parameters λ_{bound} , λ_{valid} , λ_{tIoU} , λ_{L1} and λ_{class} are set to 5, 1, 2, 5, 1, respectively. The number of queries N_0 in each *Query Set* is set to 100, and τ is set to 0.5. We train EventFormer with AdamW [28] optimizer setting transformer's learning rate to 10^{-4} , AU feature encoder's learning rate to 10^{-5} , and weight decay to 10^{-4} . Batch size is set to 8 and the number of training epochs is set to 100. All models are trained on two NVIDIA Tesla V100 GPUs.

B. Comparison among Schemes

We classify AU event detection schemes into three categories, which use frame-level (Frame2Event), unit-level (Unit2Event), and video-level (Video2Event) results to detect AU events respectively. To demonstrate the effectiveness of EventFormer, which follows the scheme of Video2Event, we implement two methods following other schemes for comparison. For a fair comparison, all methods including EventFormer apply the same AU feature encoder pre-trained using frame-level AU occurrence labels.

Backbone	Method	mAP@0.3	mAP@0.4	mAP@0.5	mAP@0.6	mAP@0.7	AR@10	AR@50	AR@100	AUC
ResNet18	Frame2Event	10.03	8.97	8.07	7.17	6.22	3.83	24.15	60.15	27.34
	Unit2Event	22.09	19.52	16.71	14.53	12.54	48.22	73.83	74.51	68.17
	Video2Event (EventFormer)	33.82	29.09	24.34	20.29	16.39	51.46	62.27	68.34	60.06
ResNet34	Frame2Event	14.33	12.20	10.53	8.80	7.23	3.93	18.58	41.37	20.09
	Unit2Event	24.04	21.18	18.15	15.84	13.77	49.09	73.79	75.85	68.49
	Video2Event (EventFormer)	36.92	32.06	26.87	22.37	18.18	52.83	64.95	69.62	62.12
ResNet50	Frame2Event	16.56	14.32	12.50	10.63	8.88	4.16	18.94	40.36	20.30
	Unit2Event	24.40	22.01	19.36	17.03	14.67	50.24	73.46	76.15	68.24
	Video2Event (EventFormer)	41.41	35.79	30.10	25.00	20.32	53.59	66.72	72.31	63.76

TABLE I
COMPARISON AMONG THREE SCHEMES ON BP4D IN TERMS OF MAP@TIOU, AR@AN AND AUC.

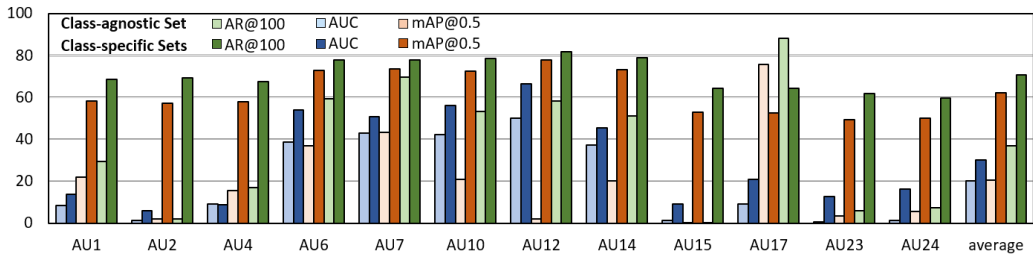


Fig. 3. A comparison between multiple class-specific sets prediction and single class-agnostic set prediction.

1) *Frame2Event Method*: Frame2Event scheme collects frame-level AU results and converts them to AU events through postprocessing such as Temporal Actionness Grouping (TAG) [29], which involves two hyper-parameters, *water level* γ and *union threshold* τ (Details in Supp.D.4). Our implementation of Frame2Event method consists of AU feature encoder and two linear layers as a classifier. Based on the predicted AU occurrence probabilities, candidate events are generated under several combinations of γ and τ . Specifically, we sample γ and τ within the range of 0.5 and 0.95 with a step of 0.05. The confidence score of each candidate event (s, e, c) is computed by averaging the probabilities of class c within segment (s, e) . Soft-NMS [30] is employed to select N_0 events for each class from the candidate events.

As shown in Table I, EventFormer outperforms Frame2Event method by a large margin in terms of mAP given any tIoU threshold, regardless of what backbone is used. Especially, EventFormer achieves a performance gain of 24.85% in mAP@0.3 than Frame2Event method using ResNet50 as backbone, which shows the superiority of EventFormer. We also notice that Frame2Event method obtains a pretty low AR given a small AN, which is because the prediction jitters due to the lack of a global view make it hard to use a set of fixed hyper-parameters to balance the trade-off between AP and AR. Such limitation reflects the necessity of maintaining a global view and detecting events directly.

2) *Unit2Event Method*: Unit2Event scheme extracts unit-level features and predicts event-related scores to generate AU events. The implementation of Unit2Event method has a

mechanism similar to [11], [10], which estimates the start and end probabilities, P_s and P_e , for each time position exhaustively, and generates an action completeness map P_c consisting of the completeness score for any event (s, e) , and the final confidence score for an event (s, e) is calculated as $P_s(s) \times P_e(e) \times P_c(s, e)$ (Details in Supp.D.5). Since such kind of method can only predict class-agnostic events, we simply make it generates C sets of P_s , P_e , and P_c , one set for each class. We adopt Soft-NMS to select N_0 events out of T^2 detected events for each class.

As shown in Table I, EventFormer outperforms Unit2Event method with any backbone in terms of mAP given any tIoU. Specifically, EventFormer achieves a performance gain of 17.01% in mAP@0.3 than Unit2Event method with ResNet50 as backbone. Since Unit2Event method generates events exhaustively, it is supposed to obtain better results in terms of AR. Although EventFormer performs a little bit worse than Unit2Event method in terms of AR given a large AN, it outperforms it in AR@10 by 3.35%, which indicates that events generated by EventFormer are of better quality.

C. Class-agnostic Set vs. Class-specific Sets

To show the superiority of viewing AU event detection as a multiple class-specific sets prediction problem instead of a single class-agnostic set prediction problem, We implement a class-agnostic version of EventFormer for comparison, which generates events with AU class labels directly and applies bipartite matching once between the ground-truth events and detected ones of all classes. From Fig. 3 we can see that the class-agnostic version obtains poor results on AU2, AU15,

Hyper-parameters	Values	mAP@0.5	AUC
#Queries in <i>Query Set</i>	10	31.78	34.77
	50	31.33	45.77
	100	30.03	62.32
Embedding Dimension	200	25.04	63.68
	128	30.22	59.65
	256	30.03	62.32
	512	24.82	61.20
d_m	1024	22.95	59.33
	3	29.39	58.67
#Encoder/decoder layers	4	29.58	59.51
	5	30.31	62.05
L	6	30.03	62.32

TABLE II
SENSITIVITY OF EVENTFORMER TO HYPER-PARAMETERS.

AU23, and AU24, of which the mAP@0.5 and AR@100 are near zero. The results variance among AU classes is huge for the class-agnostic version, while the class-specific version achieves relatively balanced results. We attribute the superiority to the binding between sets and AU classes, which is essential for stabilizing training and alleviating the variance of the results among AU classes caused by the data imbalance problem.

D. Sensitivity Analysis

We also analyze the sensitivity of EventFormer to hyper-parameters, including the number of queries in *Query Set* N_0 , embedding dimension d_m and the number of layers L of encoder and decoder, as shown in Table II. As the number of queries in *Query Set* increases, mAP decreases while AUC increases, due to the trade-off between mAP and AR. We notice that the mAP does not decrease a lot from $N_0 = 10$ to $N_0 = 100$, and AUC increases much slower when $N_0 > 100$. Thus, we choose $N_0 = 100$ for EventFormer. As for d_m , AUC reaches its peak when we set d_m to 256, while at the same time, mAP is also around its best score. As for the number of layers L , we notice that EventFormer achieves better performance with L increasing. For the balance between computing complexity and model performance, we choose $L = 6$ for EventFormer.

E. Qualitative Results

1) *Visualization of Attention in EventFormer*: To better understand how the attention mechanism takes effect in EventFormer, we visualize the attention weights of the last layer of transformer decoder in Fig. 4. The brightest parts of the attention show that the cross-attention of event transformer decoder tends to focus on the embeddings of frames where the states of AUs change. The results also show that EventFormer could capture subtle and transient appearance changes that occur in a very short duration (≤ 5 frames) and detect an event successfully, as shown in Fig. 4(a).

2) *Visualization of Detected AU Events*: Fig. 5 shows AU events detected by (a) Frame2Event method and (b) EventFormer. AU events detected by EventFormer are of

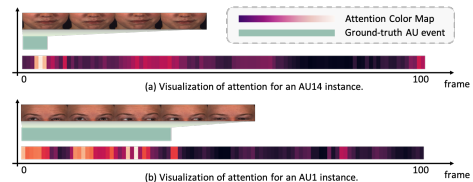


Fig. 4. Visualization of attention in EventFormer.

better quality, while AU events detected by Frame2Event method contains several false positive events with a very short duration. There is a false positive event of AU2 (Outer Brow Raiser) in Fig 5(b), and the visualized frames corresponding to this period show a process of the subject opening her eyes, during which wrinkles appeared above her eyebrow, misleading EventFormer to detect an AU2 event.

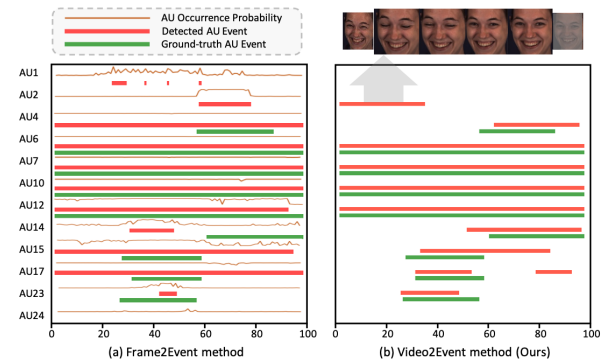


Fig. 5. Visualization of detected AU events.

VI. CONCLUSION

This paper focuses on making full use of global temporal information to directly detect AU events from a whole video sequence, which are more practical and critical in some real-world application scenarios, such as financial anti-fraud. We propose EventFormer for AU event detection, which use the mechanism of transformer to model global temporal relationships among frames, and extensive experiments show the effectiveness of our EventFormer.

REFERENCES

- [1] P. Ekman and W. Friesen, *Facial action coding system: A technique for the measurement of facial movement*, 1978.
- [2] U. Ciftci, X. Zhang, and L. Tin, "Partially occluded facial action recognition and interaction in virtual reality applications," in *ICME*. IEEE, 2017, pp. 715–720.
- [3] C. Wang and S. Wang, "Personalized multiple facial action unit recognition through generative adversarial recognition network," in *ACM MM*, 2018, pp. 302–310.
- [4] P. Tirupattur, K. Duarte, Y. S. Rawat, and M. Shah, "Modeling multi-label action dependencies for temporal action localization," in *CVPR*, 2021, pp. 1460–1470.
- [5] T. Baltrušaitis, L. Li, and L. Morency, "Local-global ranking for facial expression intensity estimation," in *ACII*, 2017, pp. 111–118.
- [6] Y. Fan, J. Lam, and V. Li, "Facial action unit intensity estimation via semantic correspondence learning with dynamic graph convolution," in *AAAI*, vol. 34, no. 07, 2020, pp. 12701–12708.

- [7] X. Song, T. Shi, Z. Feng, M. Song, J. Lin, C. Lin, C. Fan, and Y. Yuan, “Unsupervised learning facial parameter regressor for action unit intensity estimation via differentiable renderer,” in *ACM MM*, 2020, pp. 2842–2851.
- [8] K. L. Schmidt, Z. Ambadar, J. F. Cohn, and L. I. Reed, “Movement differences between deliberate and spontaneous facial expressions: Zygomaticus major action in smiling,” *Journal of nonverbal behavior*, vol. 30, no. 1, pp. 37–52, 2006.
- [9] J. F. Cohn and K. Schmidt, “The timing of facial motion in posed and spontaneous smiles,” in *Active Media Technology*. World Scientific, 2003, pp. 57–69.
- [10] Y. Chen, J. Zhang, D. Chen, T. Wang, Y. Wang, and Y. Liang, “Aupro: Multi-label facial action unit proposal generation for sequence-level analysis,” in *ICONIP*. Springer, 2021, pp. 88–99.
- [11] X. Ding, W.-S. Chu, F. De la Torre, J. F. Cohn, and Q. Wang, “Facial action unit event detection by cascade of tasks,” in *ICCV*, 2013, pp. 2400–2407.
- [12] W. Li, F. Abtahi, and Z. Zhu, “Action unit detection with region adaptation, multi-labeling learning and optimal temporal fusing,” in *CVPR*, 2017.
- [13] S. Hochreiter and J. Schmidhuber, “LSTM can solve hard long time lag problems,” in *NIPS*, 1996.
- [14] T. Simon, M. H. Nguyen, F. De La Torre, and J. F. Cohn, “Action unit detection with segment-based svms,” in *2010 IEEE Computer Society Conference on Computer Vision and Pattern Recognition*, 2010, pp. 2737–2744.
- [15] T. Simon, M. H. Nguyen, F. De La Torre, and J. F. Cohn, “Action unit detection with segment-based svms,” in *CVPR*. IEEE, 2010, pp. 2737–2744.
- [16] K. Zhao, W. Chu, and H. Zhang, “Deep region and multi-label learning for facial action unit detection,” in *CVPR*, 2016.
- [17] Y. Fan, J. Shen, H. Cheng, and F. Tian, “Joint facial action unit intensity prediction and region localisation,” in *ICME*. IEEE, 2020, pp. 1–6.
- [18] A. Vaswani, N. Shazeer, N. Parmar, J. Uszkoreit, L. Jones, A. N. Gomez, L. Kaiser, and I. Polosukhin, “Attention is all you need,” in *NIPS*, 2017.
- [19] B. Wu, C. Xu, X. Dai, A. Wan, P. Zhang, Z. Yan, M. Tomizuka, J. Gonzalez, K. Keutzer, and P. Vajda, “Visual transformers: Token-based image representation and processing for computer vision,” *arXiv preprint arXiv:2006.03677*, 2020.
- [20] N. Carion, F. Massa, G. Synnaeve, N. Usunier, A. Kirillov, and S. Zagoruyko, “End-to-end object detection with transformers,” in *ECCV*. Springer, 2020, pp. 213–229.
- [21] T. Zhao and X. Wu, “Pyramid feature attention network for saliency detection,” in *CVPR*, 2019, pp. 3085–3094.
- [22] J. L. Ba, J. R. Kiros, and G. E. Hinton, “Layer normalization,” *arXiv preprint arXiv:1607.06450*, 2016.
- [23] R. Xiong, Y. Yang, D. He, K. Zheng, S. Zheng, C. Xing, H. Zhang, Y. Lan, L. Wang, and T. Liu, “On layer normalization in the transformer architecture,” in *ICML*. PMLR, 2020, pp. 10524–10533.
- [24] H. W. Kuhn, “The hungarian method for the assignment problem,” *Naval Research Logistics Quarterly*, vol. 2, no. 1-2, pp. 83–97, 1955.
- [25] X. Zhang, L. Yin, J. F. Cohn, S. Canavan, M. Reale, A. Horowitz, P. Liu, and J. M. Girard, “Bp4d-spontaneous: A high-resolution spontaneous 3d dynamic facial expression database,” *Image and Vision Computing*, vol. 32, no. 10, pp. 692–706, 2014.
- [26] C. Lin, J. Li, Y. Wang, Y. Tai, D. Luo, Z. Cui, C. Wang, J. Li, F. Huang, and R. Ji, “Fast learning of temporal action proposal via dense boundary generator,” in *AAAI*, vol. 34, no. 07, 2020, pp. 11499–11506.
- [27] K. He, X. Zhang, S. Ren, and J. Sun, “Deep residual learning for image recognition,” in *CVPR*, 2016.
- [28] I. Loshchilov and F. Hutter, “Decoupled weight decay regularization,” *arXiv preprint arXiv:1711.05101*, 2017.
- [29] Y. Zhao, Y. Xiong, L. Wang, Z. Wu, X. Tang, and D. Lin, “Temporal action detection with structured segment networks,” in *ICCV*, Oct 2017.
- [30] N. Bodla, B. Singh, R. Chellappa, and L. S. Davis, “Soft-nms – improving object detection with one line of code,” in *ICCV*, Oct 2017.

APPENDIX

Spatial attention layer (SA) is an essential part of EventFormer to extract region-aware features focusing on local

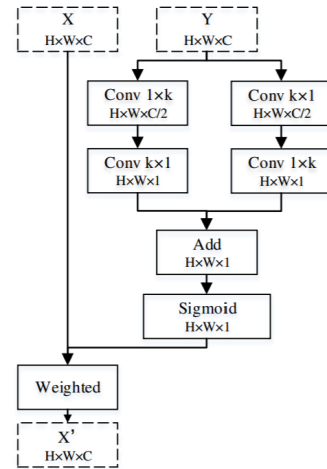


Fig. 6. The architecture of spatial attention layer in [21].

facial regions where a certain AU activates. We apply C spatial attention layers after the backbone network in AU feature encoder to learn better feature representations aware of AU-specific local facial regions, by giving each spatial location in the output feature map a different attention weight. Each spatial attention layer consists of two convolutional layers, where one’s kernel is of size $1 \times k$, and the other’s kernel is of size $k \times 1$, and we set $k = 9$ in the experiments empirically. The detailed architecture of spatial attention layer is shown in Figure 6. Each input facial image is first fed into a backbone network to obtain global feature $F_{\text{global}} \in \mathbb{R}^{d \times H_0 \times W_0}$, and then go through C spatial attention layers separately. After that, C reweighted features $F_{\text{atttn}} \in \mathbb{R}^{d \times H_0 \times W_0}$ as the output of each spatial attention layer are obtained and further mapped into $f^{\text{local}} \in \mathbb{R}^d$ through a linear layer. Finally, C region-aware local features are concatenated into $F_{\text{local}} \in \mathbb{R}^{(d \times C)}$ as a frame embedding.

The basic components of transformer encoder-decoder are Multi-layer Perceptron(MLP) block and Multi-head Attention(MHA) block. MLP block consists of two linear layers with *RELU* as activation function, and the mechanism of MHA block is given below. Residual connections [27] are added to each block.

A. Scaled Dot-Product Attention

The key part of MHA block is Scaled Dot-Product Attention, denoted by $\text{Attn}(Q, K, V)$, is computed as follows:

$$\text{Attn}(Q, K, V) = \text{Softmax}\left(\frac{(QW^Q)(KW^K)^T}{\sqrt{d_k}}\right)VW^V \quad (7)$$

Q, K and V denotes *Query*, *Key* and *Value* embeddings, and $W^Q \in \mathbb{R}^{d_m \times d_k}$, $W^K \in \mathbb{R}^{d_m \times d_k}$, $W^V \in \mathbb{R}^{d_m \times d_v}$ denote the weight matrix to compute Q, K and V respectively, where d_m is the embedding dimension and d_k and d_v are the hidden dimension for queries/keys and values respectively.

B. Multi-head Attention

Multi-head Attention(MHA) is an extension of Scaled Dot-Product Attention, in which Scaled Dot-Product Attention operations are applied h times in parallel and the output of each Scaled Dot-Product Attention operation are concatenated and mapped via a linear layer as the final output, which is called h -head attention.

MHA can be computed as follows:

$$\text{MHA}(Q, K, V) = \text{Concat}(\{\text{Attn}(Q, K, V)\}_{i=1}^h)W^O, \quad (8)$$

where $W^O \in \mathbb{R}^{hd_v \times d_m}$ is a learnable weight parameter for mapping the concatenated features of each head, and h is the number of attention heads.

All MHA blocks in transformer encoder and the first MHA block in transformer decoder takes $Q = K = V$ as input, which is called self-attention. Other MHA blocks in transformer decoder take the output of transformer encoder as K and V , and the input of decoder as Q , which is called cross-attention.

C. Positional Encoding

To maintain positional information among frames in the input video sequence, positional encodings are employed to generate corresponding positional embeddings \mathcal{P} for frame embeddings \mathcal{E} . By concatenating \mathcal{E} and \mathcal{P} together, we obtained the input queries and keys for MHA blocks in our event transformer encoder.

Specifically, we use sine and cosine functions for positional encoding to generate $\mathcal{P} = \{P_t\}_{t=1}^T \in \mathbb{R}^{T \times d_m}$, as shown in Eq. 9.

$$\begin{aligned} p_{t,2i} &= \sin(t/10000^{2i/d_m}), \\ p_{t,2i+1} &= \cos(t/10000^{2i/d_m}), 0 \leq i < \frac{d_m}{2}, \end{aligned} \quad (9)$$

where t denotes the position of each frame in a video sequence and i is the dimension of the positional encoding corresponds to a sinusoid. The periodicity of the sine and cosine function makes it easier for the model to obtain information about the relative position of different frames.

Here we provide more details of EventFormer architecture, including the formulated forward step of EventFormer encoder-decoder, and classification and regression branches.

D. EventFormer Encoder-decoder

In our EventFormer encoder-decoder, *LayerNorm* function [22] is applied before every blocks [23] to ensure a stable training period.

EventFormer encoder consists of L identical encoder layers, and each encoder layer is composed of an MHA block and an MLP block. The encoder module aims to generate refined frame embeddings with global information to the decoder for further processing. The computing procedure of each encoder layer is shown as:

$$\begin{aligned} \mathcal{E}'_l &= \text{LayerNorm}(\mathcal{E}_l), \\ \mathcal{E}''_l &= \text{MHA}([\mathcal{E}'_l, \mathcal{P}], [\mathcal{E}'_l, \mathcal{P}], \mathcal{E}'_l) + \mathcal{E}_l, \\ \mathcal{E}_{l+1} &= \text{MLP}(\text{LayerNorm}(\mathcal{E}''_l)) + \mathcal{E}''_l, 0 \leq l < L, \end{aligned} \quad (10)$$

where \mathcal{P} denotes the learned positional embeddings, and \mathcal{P} along with the input frame embeddings or the output of previous encoder layers, serve as the input of each encoder layer.

The architecture of EventFormer decoder is similar to that of EventFormer encoder, which consists of L identical decoder layers. The difference lies in that each decoder layer has two MHA blocks and one MLP block. Refined frame embeddings \mathcal{E}_L generated from the encoder, along with the queries \mathcal{Q} represented by learned positional embeddings, are then fed into the decoder as input.

The mechanism of each decoder layer is given in Eq. 11.

$$\begin{aligned} \mathcal{D}'_l &= \text{LayerNorm}(\mathcal{D}_l), \\ \mathcal{D}''_l &= \text{MHA}([\mathcal{D}'_l, \mathcal{Q}], [\mathcal{D}'_l, \mathcal{Q}], \mathcal{D}'_l) + \mathcal{D}_l, \\ \tilde{\mathcal{D}}_l &= \text{LayerNorm}(\mathcal{D}''_l), \\ \tilde{\mathcal{D}}'_l &= \text{MHA}([\tilde{\mathcal{D}}_l, \mathcal{Q}], [\mathcal{E}_L, \mathcal{P}], \mathcal{E}_L) + \mathcal{D}''_l, \\ \mathcal{D}_{l+1} &= \text{MLP}(\text{LayerNorm}(\tilde{\mathcal{D}}'_l)) + \tilde{\mathcal{D}}'_l, 0 \leq l < L, \end{aligned} \quad (11)$$

where \mathcal{Q} as one of the input of each decoder layer, is a set of learnable positional embeddings, and \mathcal{D}_0 is a placeholder as the same shape as \mathcal{Q} to keep the input dimension of each decoder layer unchanged.

E. Classification and Regression Branches

The event embeddings \mathcal{D}_L as the output of EventFormer encoder-decoder, where each feature vector $d_i \in \mathbb{R}^{d_m}$ is an embedding for a potential event φ_i , are further fed into classification and regression branches separately. The regression branch, which consists of two linear layers, predicts the start time s_i and lasting duration l_i of φ_i , and the classification branch, which consists of one linear layer, estimates a one-hot vector $\hat{p}_i \in \mathbb{R}^2$ that denotes the probabilities of the value of \tilde{c}_i , as shown in Eq. 12:

$$\begin{aligned} \hat{p}_i &= \text{softmax}(d_i.W^D), \\ [s_i, l_i] &= \text{ReLU}(d_i.W_1^R)W_2^R, \end{aligned} \quad (12)$$

where $W^D \in \mathbb{R}^{d_m \times C}$, $W_1^R \in \mathbb{R}^{d_m \times d_m}$, $W_2^R \in \mathbb{R}^{d_m \times 2}$ are learnable weight parameters for the two branches.

F. Effectiveness of Region-aware Local Features

To demonstrate the effectiveness of region-aware local features extracted by adding spatial attention layers, we conduct extensive experiments as shown in Table III. We use three backbone networks in AU feature encoder and train two models for each backbone network, one is EventFormer with spatial attention layers (w/ SA) in AU feature encoder, the other is EventFormer without spatial attention layers

Backbone	Method	mAP@0.3	mAP@0.4	mAP@0.5	mAP@0.6	mAP@0.7	AR@10	AR@50	AR@100	AUC
ResNet18	w/o SA	33.29	28.46	23.59	20.06	16.40	49.67	64.04	71.88	61.37
	w/ SA	33.82	29.09	24.34	20.29	16.39	51.46	62.27	68.34	60.06
ResNet34	w/o SA	35.84	30.52	25.25	20.96	16.60	49.15	57.56	66.33	56.30
	w/ SA	36.92	32.06	26.87	22.37	18.18	52.83	64.95	69.62	62.12
ResNet50	w/o SA	39.91	34.53	28.44	23.39	18.09	51.51	63.23	68.48	60.66
	w/ SA	41.41	35.79	30.10	25.00	20.32	53.59	66.72	72.31	63.76

TABLE III
EFFECTIVENESS OF REGION-AWARE LOCAL FEATURES.

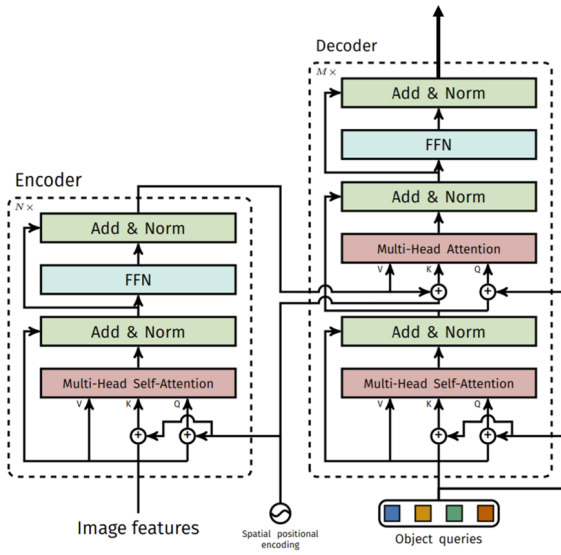


Fig. 7. Transformer architecture [20].

(w/o SA) in AU feature encoder. From Table III we can observe that EventFormer with spatial attention layers in AU feature encoder outperforms that without spatial attention layers, which illustrates the effectiveness of region-aware local feature. Since AUs cause subtle appearance changes in several local facial regions, extracting region-aware local features via spatial attention layers makes it easier to capture such appearance changes.

G. Illustration of Three Schemes for AU Event Detection

Fig. 8 shows three schemes for AU event detection. The first scheme (Frame2Event) taking advantage of the previous frame-level AU recognition works is to convert frame-level AU recognition results of all frames in a video sequence into events through postprocessing methods, as shown in Fig. 8(a). We choose TAG [29] as the post-processing method for our implementation of Frame2Event method under this scheme.

The second scheme (Unit2Event) is shown in Fig. 8(b). We implement Unit2Event method under this scheme for comparison, which predicts a confidence map, and the value in each location (s, e) satisfied $0 \leq s < e \leq T$ represents the confidence score for a potential event (s, e) starting at s and ending at e . Since such kind of method can only

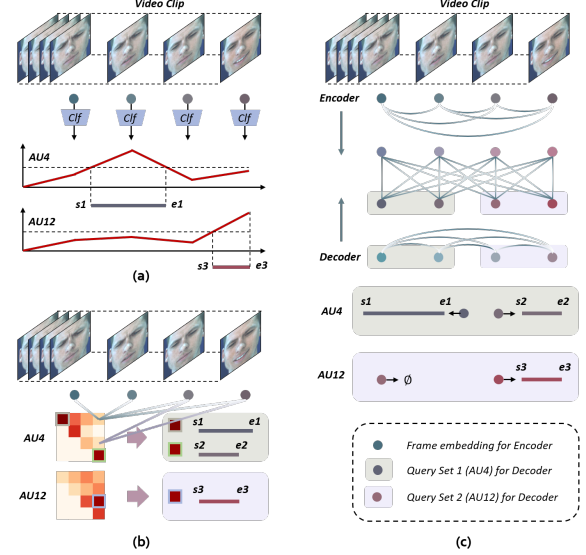


Fig. 8. Illustration of three schemes for AU event detection. (a) Frame2Event scheme. Each frame is fed to a classifier to obtain AU occurrence probabilities, a set of hyper-parameters is selected to convert the frame-level results into AU events. (b) Unit2Event scheme. Unit-level features for each frame are extracted and used to generate events in an exhaustive way. (c) Video2Event scheme. Frame embeddings are fed to event transformer encoder for embedding enhancement, and the encoder output and queries in each *Query Set* are fed to event transformer decoder for event embeddings aggregation.

predict class-agnostic results, we simply solve the problem by making it predict C confidence maps, one for each AU class. A given number of events for each AU class are picked out based on their confidence scores through Soft-NMS [30].

The third scheme (Video2Event), as shown in Fig. 8(c), is to directly detect events for each AU class simultaneously from a input video sequence. EventFormer follows this scheme by viewing AU event detection as a multiple class-specific sets prediction problem.

H. Pre-trained AU Recognition Models

For a fair comparison among the three schemes, we apply the same AU feature encoder in the implementations of each scheme and initialize AU feature encoder using the same weights. AU feature encoder with two extra linear layers added as a classifier are pre-trained using frame-level AU occurrence labels for multi-label AU recognition. We initialize AU feature encoder in the implementations under

Backbone	AU1	AU2	AU4	AU6	AU7	AU10	AU12	AU14	AU15	AU17	AU23	AU24	Avg.
ResNet18	49.3	40.1	56.9	76.0	79.4	83.9	86.8	62.8	49.1	60.4	42.9	42.7	60.9
ResNet34	54.0	45.8	53.1	70.6	78.3	82.2	84.9	58.7	45.5	61.0	48.5	44.3	60.6
ResNet50	49.5	36.4	54.9	76.4	78.1	83.7	85.7	61.6	48.0	63.5	46.8	50.2	61.2

TABLE IV
F1-SCORE OF PRE-TRAINED AU RECOGNITION MODELS.

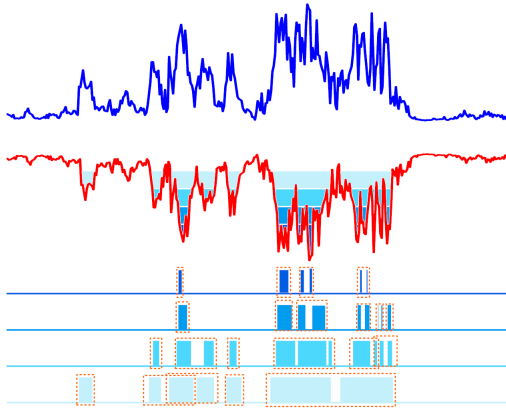


Fig. 9. Visualization of TAG process [29].

each scheme using the same pre-trained weights and fix them during training, which can be regarded as a two-stage training strategy. The performance of pre-trained AU recognition models using different backbones is listed in Table IV.

I. Details of Frame2Event Method

Temporal Actionness Grouping (TAG) applies a classic watershed algorithm to a 1D signal formed by a sequence of actionness values. Two hyper-parameters, *water level* γ and union threshold τ , are required for TAG. By horizontally mirroring the sequence of AU occurrence probabilities of each frame, a complement signal of the sequence of AU occurrence probability which looks like terrain with many basins is obtained, as shown in Fig. 9. After flooding it with different *water level* γ , some basins are filled with *water* while some higher terrain not. Adjacent basins are merged until the fraction of the total length of all basins' duration over the length of the union one's duration drops below the union threshold τ , resulting in a set of merged basins denoting events.

An illustration of our Frame2Event method is given in Fig. 10. There are mainly two kinds of problems remaining in Frame2Event method. From the case on the top of Fig. 10, we can see that different levels of the hyper-parameter γ result in different performance. However, it is hard to select an appropriate γ that satisfies getting a high recall value and high precision value at the same time, mainly because the frame-level method lacks a global view and jitters are inevitable. The case on the bottom of Fig. 10 shows that it is hard to choose a value for the other hyper-parameter τ , resulting in some false positives and events with inaccurate timing boundaries.

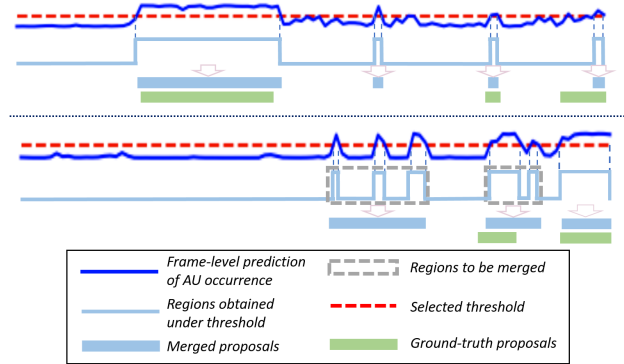


Fig. 10. Illustration of Frame2Event method [10]. In the case on the top, it is hard to select a threshold for TAG to obtain a true positive for the second ground-truth shown in green line while controlling the number of jitters the same. In the case on the bottom, the first three jitters are merged into events shown in gray bounding boxes through TAG, resulting in one false positive and one true positive of poor quality.

J. Details of Unit2Event Method

Event Feature Map Generation			
layer	output shape	layer	output shape
Conv1D	$256 \times T$	PFG	$128 \times 32 \times T \times T$
Conv1D	$128 \times T$	Conv3D	$512 \times T \times T$
Completeness Branch		Boundary Branch	
layer	output shape	layer	output shape
Conv2D	$256 \times T \times T$	Conv2D	$256 \times T \times T$
Conv2D	$256 \times T \times T$	Conv2D	$256 \times T \times T$
Conv2D	$1 \times T \times T$	Conv2D	$2 \times T \times T$

TABLE V
DETAILED ARCHITECTURE OF OUR UNIT2EVENT METHOD.

Our implementation of Unit2Event method takes the same frame embeddings \mathcal{E} as input and outputs the probabilities of each frame as start or end, and the probability of each potential event being completed, *i.e.* the completeness score of each potential event. The details of the implemented network structure can be found in Table V.

The frame embeddings $\mathcal{E} \in \mathbb{R}^{T \times d_m}$, where T is the number of frames and d_m denotes the length of each embedding, are fed into a subnet composed of several 1D convolution layers with kernel size set to 3 for further local semantic information extraction, which results in $F \in \mathbb{R}^{T \times 128}$. An event feature generation layer (PFG) [26] is applied to transfer F to $F_{mat} \in \mathbb{R}^{T \times T \times 512}$ based on the sampled

features from start region, central region, and end region. Features in each position (s, e) , where $s, e \in \mathbb{N}$ and $0 \leq s < e \leq T$, can be regarded as $f_{(s,e)} \in \mathbb{R}^{512}$ for the event starting at s and ending at e . To obtain the start and end probabilities as well as the action completeness map, F_{mat} is shared by two branches, *Completeness Branch* and *Boundary Branch*, consisting of several 2D convolution layers which are structurally similar to each other. The *Completeness Branch* outputs the action completeness map $P_c \in \mathbb{R}^{T \times T}$, and the *Completeness Branch* outputs the start and end probabilities, $P_s \in \mathbb{R}^T$ and $P_e \in \mathbb{R}^T$. The final confidence score of each potential event (s, e) is then calculated as $P_s(s) \times P_e(e) \times P_c(s, e)$ and threshold is selected to pick out candidate events with high confidence score through Soft-NMS.